Available online at www.sciencedirect.com
SCIENCE DIRECT®
Carbohydrate Research 340 (2005) 2661–2669
Carbohydrate RESEARCH

Dynamic site heterogeneity in amorphous maltose and maltitol from spectral heterogeneity in erythrosin B phosphorescence

Sonali Shirke and Richard D. Ludescher*

Department of Food Science, Rutgers, The State University of New Jersey, New Brunswick, NJ 08901-8520, USA

Received 9 May 2005; accepted 10 August 2005
Available online 5 October 2005

Abstract—We have used phosphorescence from erythrosin B (tetraiodofluorescein) dispersed in thin films of either maltose or maltitol to investigate the physical properties of these amorphous pure sugar matrixes. Intensity decays collected as a function of emission wavelength over the range from 640 to 720 nm were analyzed using a stretched exponential kinetic model in which the lifetime (τ) and the stretching exponent (β) were the physically relevant parameters. The lifetimes varied systematically with emission wavelength in both matrixes. Analysis of the temperature dependence of the lifetime at each wavelength provided an estimate of the activation energy for nonradiative quenching of the triplet state; the activation energy also varied with emission wavelength. In addition, time-resolved emission spectra exhibited a blue shift with time following excitation. These data support a photophysical model in which probes are distributed among sites that vary in terms of overall molecular mobility and in which sites with lower rates of dipolar relaxation also have lower rates of collisional quenching of the erythrosin triplet state. The amorphous matrix of both maltose and maltitol in both the glass and the melt state is thus characterized by dynamic site heterogeneity in which different sites vary in terms of their overall molecular mobility.

Keywords: Maltose; Maltitol; Amorphous solid; Glass; Glass transition; Dynamic heterogeneity; Phosphorescence; Spectral heterogeneity

1. Introduction

Although devoid of long range, crystalline order, supercooled liquids and solids composed of either small molecules or polymers exhibit local structural features characterized by sufficiently different local packing densities or noncovalent interactions to generate wide variations in the rates of molecular mobility. Research integrating data from a variety of primarily spectroscopic techniques[1–4] indicate that a variety of supercooled materials—liquids and solids, small molecules, and polymers—exhibit heterogeneity in both space and time: at any given time the molecular dynamics at sites spatially distributed throughout the material can differ significantly while at any given spatial site the molecular dynamics can fluctuate significantly as a function of time. Much effort has been expended to characterize this spatial and temporal heterogeneity, either by determining the variation in the rates of mobility within the matrix or by determining the size or fluctuation times characteristic of these dynamically distinct sites.[5–7] The implications of spatial and temporal heterogeneity in amorphous solids for practical issues in polymer science and food technology, for example, are only now being discussed,[8–10] in part because the dynamic heterogeneity of amorphous carbohydrates and proteins is poorly characterized.

A few studies suggest that this dynamic heterogeneity is also characteristic of polyols. Evidence for dynamic heterogeneity in D-glucitol has come from spectroscopic measurements of lower than average β relaxation rates within a sub-ensemble of molecules selected by means of a spectroscopic filter in dielectric hole-burning experiments.[11] Earlier studies of diffusion in highly viscous aqueous sucrose[12] and maltose[13] had indicated that the translational self diffusion coefficient follows a weaker

* Corresponding author. Tel.: +1 732 932 9611x231; fax: +1 732 932 6776; e-mail: ludescher@aesop.rutgers.edu

0008-6215/$ - see front matter © 2005 Elsevier Ltd. All rights reserved.
doi:10.1016/j.carres.2005.08.015

than expected temperature dependence at temperatures near and above T_g. Although not posited by the original investigators, this behavior has recently been interpreted in terms of a physical picture of heterogeneous dynamics.[2,4] The spatial extent of these localized dynamic regions in D-glucitol have been estimated at 2.5 nm using NMR[14] and 3.6 nm using DSC.[6] Clearly, the generality of this behavior requires further investigation.

We have recently demonstrated that phosphorescence emission from erythrosin B (tetraiodofluorescein) provides a novel method of monitoring site heterogeneities in amorphous solid sucrose and gelatin.[15,16] The evidence for such dynamic heterogeneities comes from systematic variations in the triplet state lifetime across the emission band as well as systematic blue shifts in the emission spectra with time following excitation. We report here that erythrosin B also displays comparable spectral heterogeneity in thin films of amorphous maltose and maltitol, suggesting that such dynamic site heterogeneities are a general property of amorphous sugars.

2. Results

2.1. Wavelength dependence of phosphorescence lifetimes

Phosphorescence intensity decays from erythrosin B dispersed in amorphous maltose and maltitol at probe:sugar ratios of $0.8{:}10^4$ were collected as a function of emission wavelength and temperature; intensity decays collected at the blue (640 nm) and red (720 nm) edges of the erythrosin B phosphorescence emission band are plotted in Figure 1. The intensity transients collected at the red edge of the emission spectrum (720 nm) decayed faster than those collected at the blue edge (640 nm) both in maltose at 20 °C and in maltitol at −25 °C. Similar variation in the decay kinetics with emission wavelength has been reported previously for this probe in amorphous sucrose[15] and gelatin[16] and for a similar xanthene probe, eosin, in amorphous sucrose at ambient temperatures,[17] and in glycerol at cryogenic temperatures.[18]

Decays were fit to a stretched exponential decay model (Eq. 3) in which the Kohlrausch–Williams–Watts lifetime[19] (τ) and the stretching exponent[20] (β) are the physically meaningful parameters. All erythrosin B intensity decays collected as a function of emission wavelength from 640 to 720 nm and temperature from −25 to 100 °C in both maltose and maltitol were well fit using a stretched exponential decay model, giving $R^2 \geqslant 0.99$ and modified residuals plots that varied randomly about zero amplitude. The variation of τ and β with emission wavelength are plotted in Figures 2 and 3 at various temperatures between −25 and 100 °C. In maltose, the lifetimes at −25 °C varied from a high of 0.73 ms at 640 and 660 nm to a low of 0.57 ms at 720 nm; lifetimes also decreased monotonically with increasing wavelength at −10 °C (Fig. 2a). At 0 °C and above, however, lifetimes increased at the blue edge to a maximum at 660–670 nm and then decreased at higher wavelengths. In maltitol, the lifetimes decreased monotonically at −25 and −10 °C, but at higher temperatures were essentially constant or at a few temperatures (20, 30, and 50 °C) increased with increasing wavelength (Fig. 2b).

The variation in lifetime can only reflect variations in the underlying photophysical rate constants as a function of emission wavelength (Eq. 3, Section 4). As discussed in detail in our previous study of erythrosin B in amorphous sucrose, any physically relevant variations in k_{RP} due its dependence on ν^3 or k_{TS1} due to variations in ΔE_{TS} would generate a systematic increase in lifetime with emission wavelength at all temperatures.[15] It thus seems probable that the variations in lifetime with emission wavelength reflect variations in the nonradiative rate constant k_{TS0} such that probes with blue-shifted emission have smaller values of k_{TS0} and probes with red-shifted emission have larger values of k_{TS0}. Arrhenius analysis of the temperature dependence of the rate constant k_P ($= 1/\tau$) at each wavelength provides an estimate of the apparent activation energy (E_A) for nonradiative quenching (k_{TS0}). These values for maltose and maltitol in the glass at low and in the melt at high temperature are plotted in Figure 4.

The activation energy for nonradiative quenching was about threefold higher in the melt at high temperature than in the glass at low temperature in both maltose and maltitol. Values in maltose varied from 1.8 to 4.4 kJ mol^{-1} at low and from 8.6 to 12.1 kJ mol^{-1} at high temperature. Although E_A was higher at short wavelength in the glass, there was no consistent variation with wavelength in the melt. In maltitol, on the other hand, E_A varied systematically with emission wavelength in both the glass and the melt, increasing from 2.0 kJ mol^{-1} at 720 nm to 7.5 kJ mol^{-1} at 640 nm at low temperature and from ∼10 kJ mol^{-1} at 710–720 nm to ∼19.5 kJ mol^{-1} at 640–650 nm at high temperature. The trend seen here, in which E_A decreased with emission wavelength in maltose glass and in maltitol glass and melt, is similar to that seen in erythrosin B in amorphous sucrose where E_A decreased with emission wavelength in both the glass and the melt.[15]

The variation of the stretching exponent (β) with emission wavelength for both maltose and maltitol at several temperatures is plotted in Figure 3. The stretching exponent is a measure of the kinetic heterogeneity in the intensity decays; a value of 1 indicates a single exponential decay (and thus no dynamic heterogeneity), while values less than 1 indicate increasing width of an asymmetric lifetime distribution.[20] For erythrosin B in maltose at −25 °C, β increased with increasing wavelength from a low of 0.79 at 640 nm to a high of 0.90

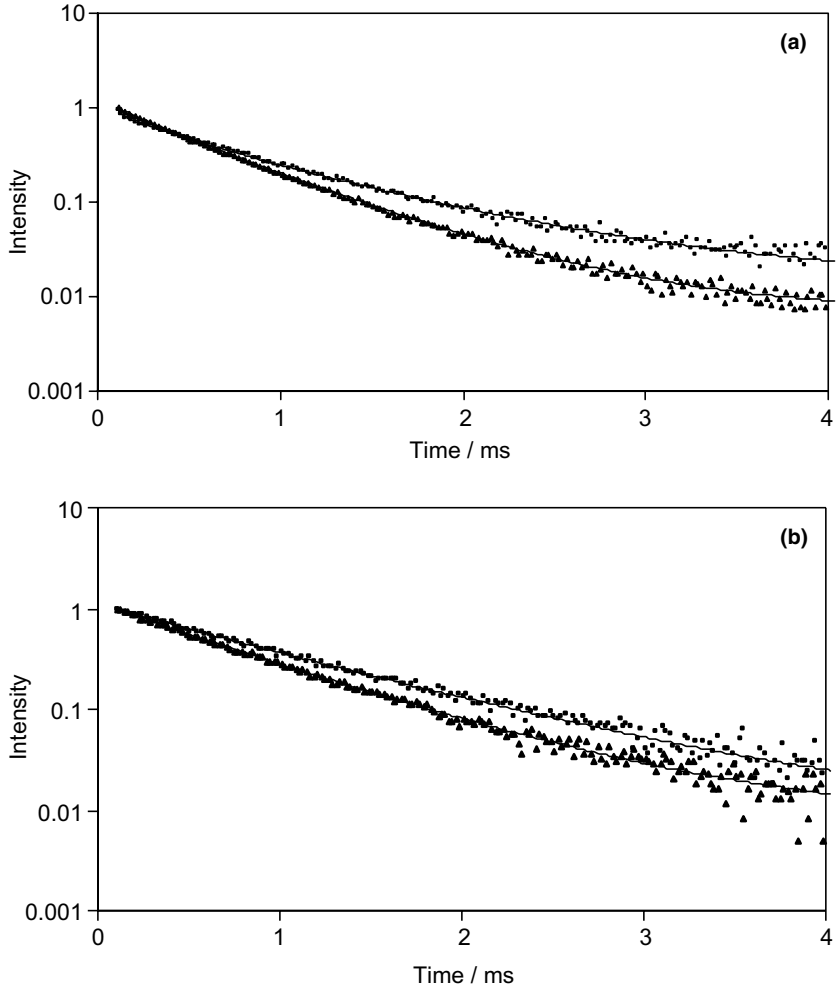

Figure 1. Phosphorescence emission intensity decay of erythrosin B dispersed in amorphous maltose at 20 °C (a) and in amorphous maltitol at −25 °C (b). Emission was collected with 530 nm excitation and emission wavelength of either 640 nm (■) or 720 nm (▲); decay curves were normalized to the intensity at time zero. The smooth curves through the data reflect fits to a stretched exponential decay model (Eq. 3, Section 4) using values of τ and β of 0.566 ms and 0.797 for maltose at 640 nm, 0.487 ms and 0.886 for maltose at 720 nm, 0.838 ms and 0.930 for maltitol at 640 nm, and 0.648 ms and 0.915 for maltitol at 720 nm.

at 680 nm and above. A similar trend of increasing β with increasing wavelength was seen at all temperatures up to 100 °C. In maltitol, however, the trends in β were less uniform at the blue edge of the emission band at 640 and 660 nm but were essentially constant at higher wavelength.

2.2. Time-resolved phosphorescence emission spectra

The variations in phosphorescence lifetime with emission wavelength suggested that long lifetime chromophores have blue-shifted phosphorescence emission and short lifetime chromophores have red-shifted emission. This prediction was tested by collecting time-resolved emission spectra for erythrosin B in amorphous maltose and maltitol as a function of delay time. These spectra, collected over a 0.5 ms window with time delays of 0.1, 0.4, 0.7, 1.1, 1.5, 2.0, and 2.5 ms are plotted in Figure 5. At short time (0.1 ms delay) the spectrum reflected emission from all chromophores (weighted by their absorbance and inverse lifetime); at long time (2.5 ms delay), however, the measured spectrum only reflected emission from long lived chromophores. The emission peak frequency (ν_P) and bandwidth (Γ_P) for these spectra (calculated using Eq. 1) are plotted versus delay time in Figures 6 and 7, respectively.

The emission frequency shifted to higher energy (blue shifted) with increasing delay time in both maltose and maltitol; these shifts were approximately linear in time and of consistent magnitude ($\sim$200 cm^{-1}) at all temperatures measured from −10 to 100 °C in maltose and from −10 to 50 °C in maltitol (Fig. 6). Except for data collected at 100 °C in maltose, all curves were approximately parallel in both sugars; vertical shifts with temperature reflected additional stabilization of the triplet state at higher temperature due to increasing dipolar relaxation rate.[15,21] These data provide independent evidence that the emission from erythrosin B in these

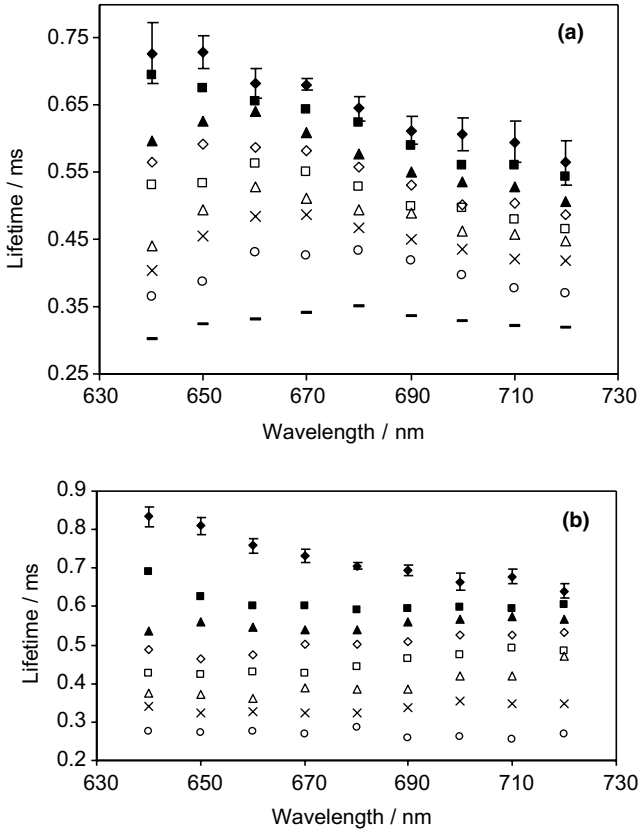

Figure 2. Effect of emission wavelength on the erythrosin B phosphorescence lifetimes in amorphous maltose (a) and maltitol (b) determined from analysis using a stretched exponential model (see Section 4). Data collected at −25 °C (♦), −10 °C (■), 0 °C (▲), 20 °C (◊), 35 °C (□), 50 °C (△), 65 °C (×), 80 °C (○), and 100 °C (—) for maltose and −25 °C (♦), −10 °C (■), 10 °C (▲), 20 °C (◊), 30 °C (□), 50 °C (△), 70 °C (×), and 80 °C (○) for maltitol. For clarity, error bars are plotted for −25 °C data only; errors at other temperatures were comparable.

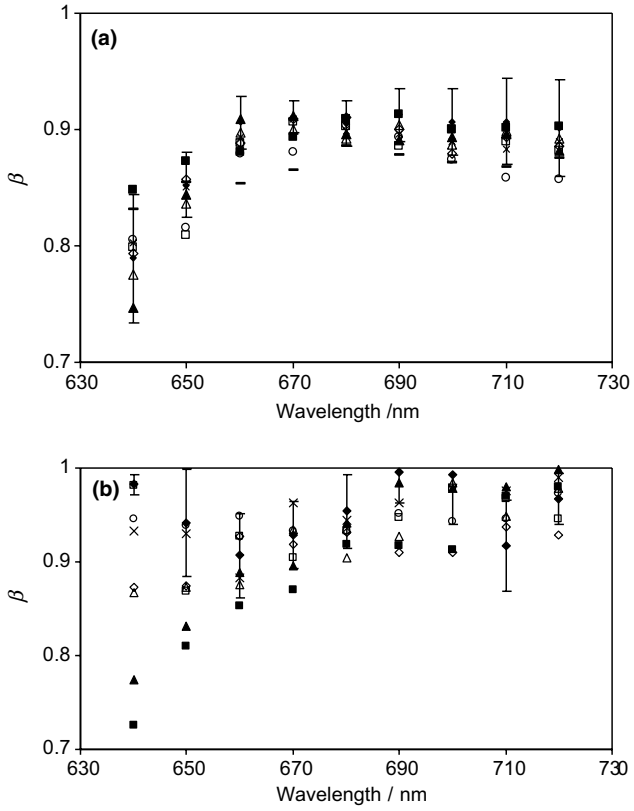

Figure 3. Effect of emission wavelength on the stretching exponent (β) characterizing the intensity decay transients of erythrosin B phosphorescence in amorphous maltose (a) and maltitol (b) determined from analysis using a stretched exponential model (see Section 4). Data collected at −25 °C (♦), −10 °C (■), 0 °C (▲), 20 °C (◊), 35 °C (□), 50 °C (△), 65 °C (×), 80 °C (○), and 100 °C (—) for maltose and −25 °C (♦), −10 °C (■), 10 °C (▲), 20 °C (◊), 3 °C (□), 50 °C (△), 70 °C (×), and 80 °C (○) for maltitol. For clarity, error bars are plotted for −25 °C data only; errors at other temperatures were comparable.

amorphous sugar matrixes is spectrally correlated such that probes in environments with shorter lifetimes have red-shifted emission spectra and probes in environments with longer lifetimes have blue-shifted emission spectra.

Analysis of the emission bandwidth Γ_P indicated that there was no consistent change with increasing delay time for erythrosin B in maltose (Fig. 7a) but a consistent increase in Γ_P with delay time in maltitol (Fig. 7b). At all temperatures measured, Γ_P increased ~15% in maltitol over the range from 0.1 to 2.5 ms delay time, suggesting that the extent of inhomogeneous broadening was larger for chromophores with blue-shifted emission spectra in maltitol but not maltose.

3. Discussion

We propose that the triplet state photophysics of erythrosin within amorphous maltose and maltitol are modulated primarily by two dynamic properties of the matrix (considered as a solvent): dipolar relaxations that lower the energy of the excited triplet state and molecular motions that quench the excited triplet state. Although these dynamic properties modulate the emission energy and lifetime of nearly all luminescent molecules,[23,24] they are only observable on the sub-nanosecond time scale in low viscosity liquids[23] and are thus usually averaged out and do not give rise to spectral heterogeneities. Due to the extremely low rates of molecular mobility within amorphous sugars, rates significantly lower than the rate of phosphorescence emission, variations in the rates of molecular mobility throughout the matrix can generate the spectral heterogeneities in phosphorescence reported here. Such a proposal generates, we believe, a consistent model for the triplet-state photophysics of erythrosin in amorphous sugars while providing insight into their solid-state biophysics. The spectral heterogeneities seen in erythrosin B phosphorescence in amorphous maltose and maltitol are quite similar to those

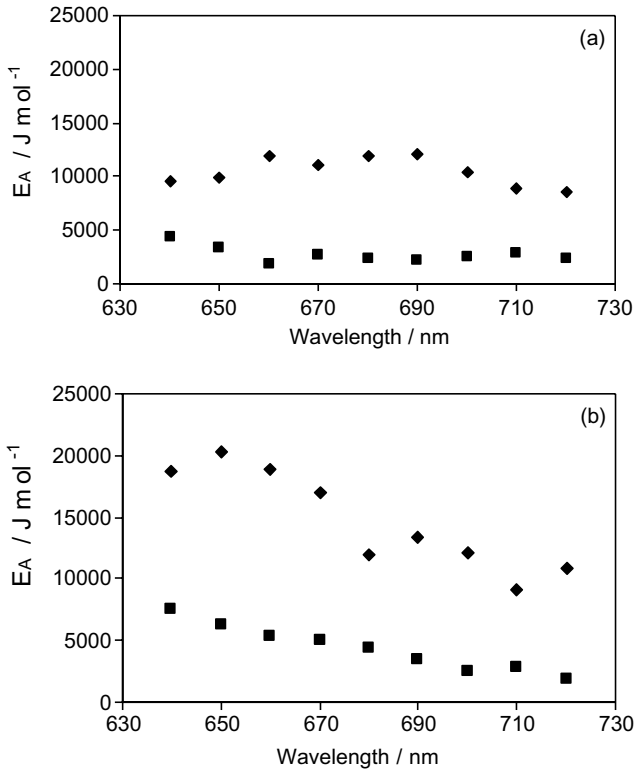

Figure 4. Variation of activation energy (E_A) for quenching of phosphorescence lifetime of erythrosin B in amorphous maltose (a) and maltitol (b) at temperatures below (■) and above (♦) the sugar and sugar alcohol glass transition temperatures.

reported previously for the same probe in amorphous sucrose[15] and gelatin.[16]

A decrease in lifetime across the emission band is not consistent with a standard relaxation model in which longer lifetime probes have red-shifted emission due to more extensive dipolar relaxation around the longer lived excited states.[22–24] However, this decrease in lifetime is consistent with a dynamic site heterogeneity model in which probes are distributed among sites within the matrix that differ in terms of their molecular mobility.[15] In this model, probes with blue-shifted emission have higher energy triplet states and are thus in sites with lower dipolar relaxation rates while probes with red-shifted emission have lower energy triplet states and are thus in sites with faster dipolar relaxation rates. In addition, probes in sites with blue-shifted emission have longer lifetimes and thus have smaller values of k_{TS0} while probes in sites with red-shifted emission have shorter lifetimes and thus larger values of k_{TS0}.

The magnitude of k_{TS0} reflects both internal factors related to the manner in which the excited T_1 state of erythrosin B is vibrational coupled to the S_0 ground state as well as external factors related to the manner in which the ground state vibrational energy of the excited probe can dissipate into the surrounding matrix.[25,26] Because the efficiency of this vibrational coupling is related to the overall viscosity of the matrix,[27] the magnitude of k_{TS0} provides a direct measure of matrix mobility. Blue-shifted sites thus have lower rates of those molecular collisions that dissipate the vibrational energy of the probe while red-shifted sites have faster rates for these molecular collisions.

In addition, red-shifted sites appear to have (in general) lower activation energies for molecular collisions that promote excited state quenching. The magnitude of the activation energy in hydroxylated solvents has been related to the size of the reorienting unit that controls the relaxation rate.[28] Higher values of E_A thus indicate that the molecular collisions that activate nonradiative quenching in these sugar matrixes involve larger cooperative units; that is, that collisional quenching involves the collective motion of larger molecular groups. Because the activation energy is larger in the melt than in the glass, molecular mobility leading to collisional quenching in both maltose and maltitol thus involves the collective motions of smaller, more localized molecular groups within the glass and the collective motions of larger, less localized molecular groups within the melt. Furthermore, the molecular collisions leading to quenching at blue-shifted sites appear to involve the collective motion of larger groups of molecules in both the glass and the melt.

Since the fit values of the stretching exponent β vary in the range from 0.8 to 0.9, erythrosin B molecules in both maltose and maltitol appear to be distributed among a continuum of matrix sites that differ in overall matrix mobility. Such a continuous distribution, rather than discrete classes of sites, is compatible with the known properties of amorphous solids.[29,30] The increase in β across the emission band indicates that blue-shifted sites exhibit a broader distribution of decay times, and thus a broader distribution of k_{TS0} values and thus rates of collisional mobility, than red-shifted sites. The magnitude of β for erythrosin B in both sucrose[15] and in maltose and maltitol[21] is higher in the glass where the lifetime is higher, and lower in the melt where the lifetime is lower; since β is low at the blue edge of the emission where τ is high, there does not appear to be any specific physical linkage between β and τ for this probe. It thus appears that although blue-shifted sites have, on average, lower molecular mobility, they also display a broader distribution of dynamic environments than red-shifted sites. This phenomenon may be related to the complexity of the dynamic landscape of amorphous materials. Blue-shifted sites have lower rates of dipolar relaxation; in general, these sites also have lower rates of mobility for collisional quenching. It is possible, however, that the physical coupling between dipolar relaxation modes and collisional quenching modes is not strict and that some of the blue sites are actually more mobile for these collisional modes than others. The result would be the observed variation of β across the emission band.

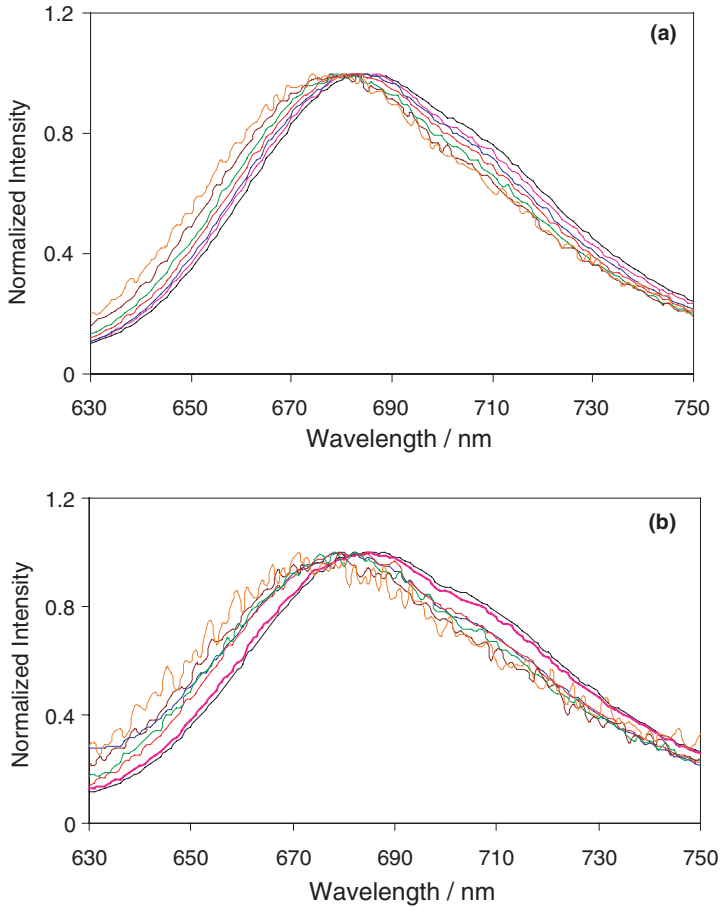

Figure 5. Phosphorescence emission spectra for erythrosin B in amorphous maltose (a) and maltitol (b) collected as a function of delay time of 0.1 ms (black), 0.4 ms (purple), 0.7 ms (blue), 1.1 ms (red), 1.5 ms (green), 2.0 ms (brown), and 2.5 ms (orange) (spectra plotted from right to left) at 20 °C. See text for details.

The following photophysical model thus seems appropriate to describe how this probe monitors the physical state of amorphous solid maltose and maltitol. Erythrosin B probes are distributed among a continuum of matrix environments ranging from blue-shifted (blue) to red-shifted (red) sites. Blue sites have lower dipolar relaxation rates, lower collisional quenching rates, higher activation energies for collisional quenching, and greater variability in the rates of collisional quenching. Blue sites thus appear to be physical regions of the amorphous matrix organized into larger aggregates of more strongly interacting sugar molecules that have lower overall molecular mobility, probably due to more extensive hydrogen bonding. Red sites, on the other hand, have faster dipolar relaxation rates, faster collisional quenching rates, lower activation energies for collisional quenching, and less variability in the rates of collisional quenching. Red sites thus appear to be physical regions of the amorphous matrix organized into smaller aggregates of weakly interacting sugar molecules that have higher overall mobility, probably due to less extensive hydrogen bonding. Although little information is available about their temporal and spatial continuity from this study, these regions must have persistence times longer than the excited triplet-state lifetime of 0.6–0.8 ms and spatial extents larger than the linear dimension of an erythrosin molecule (~1 nm).[31]

These phosphorescence data thus support a physical model for dynamic site heterogeneities within amorphous maltose and maltitol that appears consistent with the physical model generated for supercooled liquids and amorphous polymers both below and above the glass transition temperature.[1–4] Given the similar dynamic behavior for erythrosin B in amorphous sucrose[15] and in amorphous lactose and lactitol,[32] and for eosin in glycerol at cryogenic temperature,[18] the existence of such dynamic site heterogeneities may be a consistent feature of the amorphous state of solid sugars, sugar alcohols, and perhaps other polyols. Since amorphous carbohydrates such as sucrose and starch form the bulk of many solid foods, while high concentrations of amor-

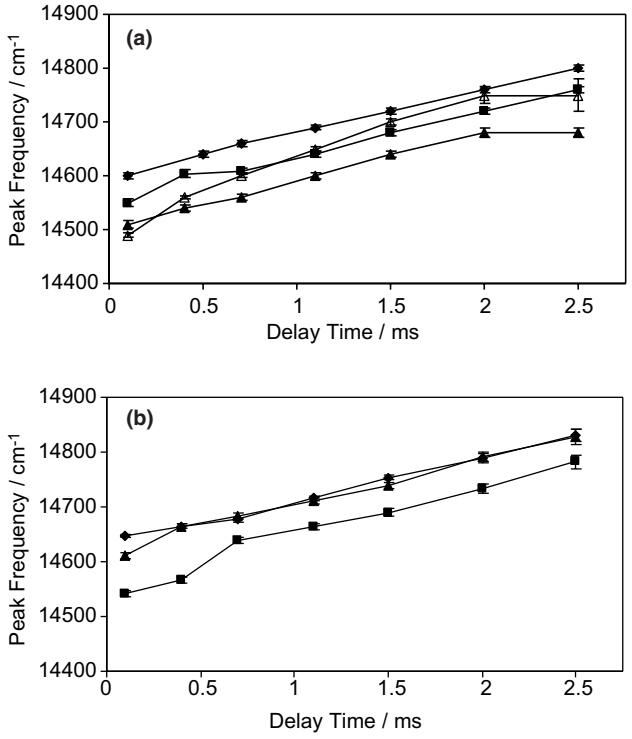

Figure 6. Evolution of phosphorescence emission peak frequency ν_P with time following excitation in amorphous maltose (a) at −10 °C (◆), 20 °C (■), 60 °C (▲), and 100 °C (Δ) and in amorphous maltitol (b) at −10 °C (♦), 20 °C (■), and 50 °C (▲).

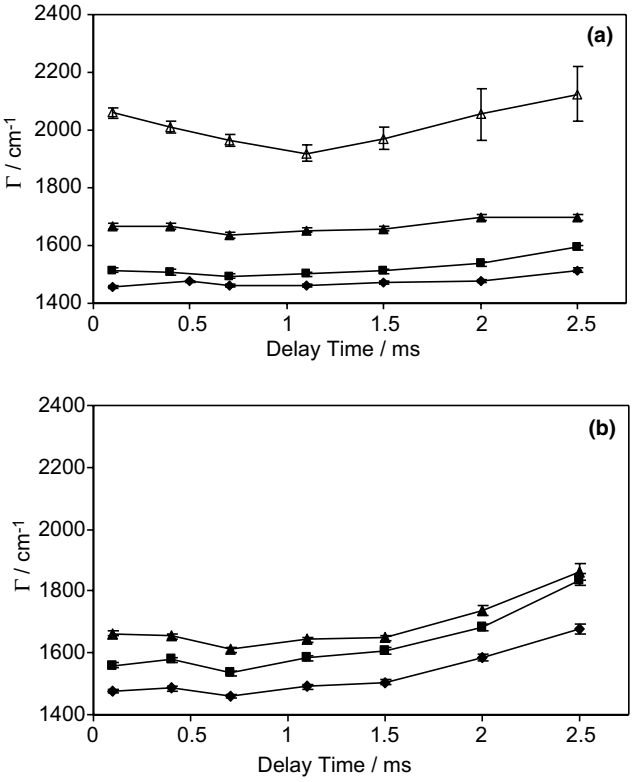

Figure 7. Evolution of phosphorescence emission bandwidth Γ_P with time following excitation in amorphous maltose (a) at −10 °C (◆), 20 °C (■), 60 °C (▲), and 100 °C (△) and in amorphous maltitol (b) at −10 °C (♦), 20 °C (■), and 50 °C (▲).

phous sucrose and trehalose matrixes in plants and other organisms protect against desiccation,[43] the implications of these dynamic heterogeneities for stability and viability clearly need investigation. Given the importance of matrix mobility for chemical reactivity and physical change,[10] dynamic site heterogeneity may result in regions within the matrix having distinctly different rates for chemical reactions such as oxidation and Maillard browning or for physical processes such as crystallization. Such heterogeneities may be especially important under conditions where the matrix is a supercooled liquid or rubber, giving rise to local 'hot spots' where the rates of reaction are significantly (perhaps as much as 10- to100-fold) higher than the matrix average.[2] The presence of such high mobility regions would be especially important for physical processes such as crystallization whose rates are controlled by nucleation.

4. Experimental

4.1. Sample preparation

The sugars maltose and maltitol (Sigma–Aldrich, St. Louis, MO), with minimum purity of 98% were dissolved in deionized water at a concentration equivalent to 66–68° Brix (wt % sucrose) as measured with a refractometer (NSG Precision Cells, Inc., Farmingdale, NY). The free acid of erythrosin B (tetraiodo fluorescein, Ery B) (Molecular Probes, Eugene, OR) was dissolved in spectrophotometer grade *N*,*N*-dimethylformamide (DMF) to make a 10 mM solution; an aliquot from this solution was added to each of the sugar and sugar alcohol solutions to obtain a solution with dye–sugar molar ratio of $0.8{:}10^4$.

An aliquot (15 μL) of dye–sugar solution was spread on a clean quartz slide 3 cm × 1.35 cm (NSG Precision Cells), which was then dried for 5 min under a 1600 W hairdryer (Vidal Sassoon, New York, NY). This method dried the films quickly without crystallization and heated the slide to ~88 °C (as measured by a thermocouple probe). The thickness of the films ranged from 10 to 40 μm as measured by micrometer (Mitutoyo Corp., Japan). The slides were stored in a desiccator containing P_2O_5 and DrieRite (DrieRite, Xenia, OH) for at least 4 days prior to any luminescence measurements. The slides were checked for crystallization under crossed polarizers using a Nikon Type 102 dissecting microscope (Nikon, Inc., Japan).

The glass transition temperature (T_g) for maltose and maltitol were determined by averaging values from the literature; T_g was 93 ± 5 °C for maltose[33–37] and 39 ± 1 °C for maltitol.[33,38,39]

4.2. Luminescence measurements and data analysis

All luminescence data were collected using a Cary Eclipse Fluorescence Spectrophotometer (Varian Instruments, Walnut Creek, CA). A slide was fitted diagonally into a standard fluorescence cuvette and was flushed with N_2 gas for at least 15 min prior to making measurements (O_2 is a contact quencher of the triplet state). The temperature was controlled using a TLC 50 thermoelectric heating/cooling system (Quantum Northwest, Spokane, WA). For measurements below room temperature, the outside of the cuvette was flushed with dry air to eliminate moisture condensation.

Phosphorescence emission spectra as a function of delay time following excitation at 500 nm (bandwidth 20 nm) were collected from 620 to 750 nm (bandwidth 10 nm). The emission intensity was collected from a single lamp flash over a 0.5-ms gate window following a delay time that varied from 0.1 to 2.5 ms; 10 cycles of excitation were averaged. Phosphorescence spectra were converted to intensity versus frequency (cm^{-1}) and analyzed to obtain the peak frequency (ν_m) and spectral bandwidth (Γ, full width at half maxima) using a lognormal function ($I(\nu)$).[40]

$$I(\nu) = I_o \exp\{-\ln(2)[\ln(1 + 2b(\nu - \nu_m)/\Delta)/b]^2\}, \quad (1)$$

I_o, ν_m, b, and Δ are the peak intensity, peak frequency, asymmetry parameter, and width parameter, respectively, for the emission band, and the bandwidth (Γ) of the emission band was related to the width and asymmetry parameters

$$\Gamma = \Delta \sinh(b)/b. \quad (2)$$

To obtain intensity decays of Ery B in maltose and maltitol as a function of emission wavelength, the samples were excited at 530 nm (bandwidth 20 nm) and emission collected as a function of emission wavelength from 640 to 720 nm (bandwidth 20 nm) over the temperature range from −25 to 100 °C. Samples were equilibrated for 5 min at each temperature before collecting data. The intensity was collected as a function of time following the lamp flash over a total window of 4 ms following a delay time of 0.1 ms and using a gate time of 0.02 ms; 10 cycles were summed to get a single decay. The intensity transients ($I(t)$) were analyzed using a stretch-exponential decay function[15,16,24]

$$I(t) = I(0) \exp[-(t/\tau)^{\beta}] + \text{constant}, \quad (3)$$

where $I(0)$ is the initial intensity at time zero, τ is the Kohlrausch–Williams–Watts lifetime[19] and β is the stretching exponent. The appropriateness of this decay model for Ery B in amorphous sugars is discussed at length in Pravinata et al.[15] Data analysis was done using the program NFIT (Island Products, Galveston, TX) using a nonlinear least squares algorithm that varies the adjustable parameters to minimize the mean square sum of deviations. All fits gave R^2 values in the range of 0.99–1.0 and modified residuals ((data − fit)/data$^{1/2}$) plots that varied randomly about zero.

The measured emission rate for phosphorescence ($k_P = 1/\tau$) is the sum of all possible de-excitation rates for the triplet state T_1[41]

$$k_P = k_{RP} + k_{TS0} + k_{TS1}, \quad (4)$$

where k_{RP} ($= 41\ s^{-1}$)[41,42] is the rate of phosphorescence emission to the ground state S_0, k_{TS1} is the rate of thermally activated reverse intersystem crossing from the excited triplet T_1 to the excited singlet S_1 and k_{TS0} is the rate of intersystem crossing from T_1 to S_0 (the rate of nonradiative quenching of the triplet state). Oxygen quenching is assumed negligible due to the elimination of oxygen. Under our experimental conditions, the magnitude of k_{TS1} made a minor contribution ($\leqslant \sim 15\%$) to the overall magnitude of k_P;[15,21] Arrhenius analysis of $k_P(T)$ thus provided a reasonable estimate of the activation energy of collisional quenching (k_{TS0}).

Acknowledgements

This research was supported by a Grant from the National Research Initiative of the United States Department of Agriculture (#2002-01585).

References

1. Sillescu, H. *J. Non-Cryst. Solids* **1999**, *243*, 81–108.
2. Ediger, M. D. *Annu. Rev. Phys. Chem.* **2000**, *51*, 99–128.
3. Sillescu, H.; Böhmer, R.; Diezemann, G.; Hinze, G. *J. Non-Cryst. Solids* **2002**, *307–310*, 16–23.
4. Richert, R. *J. Phys.: Condens. Mat.* **2002**, *14*, R738–R803.
5. Schmidt-Rohr, K.; Spiess, H. W. *Phys. Rev. Lett.* **1991**, *66*, 3020–3023.
6. Hempel, E.; Hempel, G.; Hensel, A.; Schick, C.; Donth, E. *J. Phys. Chem. B* **2000**, *104*, 2460–2466.
7. Wang, C.-Y.; Ediger, M. D. *J. Phys. Chem. B* **1999**, *103*, 4177–4184.
8. Thurau, C. T.; Ediger, M. D. *J. Chem. Phys.* **2002**, *116*, 9089–9099.
9. Thurau, C. T.; Ediger, M. D. *J. Chem. Phys.* **2003**, *118*, 1996–2004.
10. Le Meste, M.; Champion, D.; Roudaut, G.; Blond, G.; Simatos, D. *J. Food Sci.* **2002**, *67*, 2444–2458.
11. Richert, R. *Europhys. Lett.* **2001**, *54*, 767–773.
12. Champion, D.; Hervet, H.; Blond, G.; Le Meste, M.; Dimatos, D. *J. Phys. Chem. B* **1997**, *101*, 10674–10679.
13. Parker, R.; Ring, S. G. *Carbohydr. Res.* **1995**, *273*, 147–155.
14. Qiu, X.-H.; Ediger, M. D. *J. Phys. Chem. B* **2003**, *107*, 459–464.
15. Pravinata, L. C.; You, Y.; Ludescher, R. D. *Biophys. J* **2005**, *88*, 3551–3561.
16. Lukasik, K. V.; Ludescher, R. D. *Food Hydrocolloids* **2005**, *20*, 88–95.
17. Pravinata, L. C. M.S. Thesis, Rutgers, The State University of New Jersey, New Brunswick, NJ, 2003.

18. Pastukhov, A. V.; Khudyakov, D. V.; Vogel, V. R.; Kotelnikov, A. I. *Chem. Phys. Lett.* **2001**, *346*, 61–68.
19. Williams, G.; Watts, D. C. *Trans. Faraday Soc.* **1970**, *66*, 80–85.
20. Lindsey, C. P.; Patterson, G. D. *J. Chem. Phys.* **1980**, *73*, 3348–3357.
21. Shirke, S.; Ludescher, R. D. *J. Phys. Chem. B* **2005**, *109*, 16119–16126.
22. Ware, W. R.; Lee, S. K.; Brant, G. J.; Chow, P. P. *J. Chem. Phys.* **1971**, *54*, 4729–4737.
23. Stratt, R. M.; Maroncelli, M. *J. Phys. Chem.* **1996**, *100*, 12981–12996.
24. Richert, R. *J. Chem. Phys.* **2000**, *113*, 8404–8429.
25. Papp, S.; Vanderkooi, J. M. *Photochem. Photobiol.* **1989**, *49*, 775–784.
26. Fischer, C. J.; Gafni, A.; Steele, D. G.; Schauerte, J. A. *J. Am. Chem. Soc.* **2002**, *124*, 10359–10366.
27. Strambini, G. B.; Gonnelli, M. *Chem. Phys. Lett.* **1985**, *115*, 196–200.
28. Kauzmann, W. *Rev. Mod. Phys.* **1942**, *14*, 12–44.
29. Zallen, R. *The Physics of Amorphous Solids*; John Wiley and Sons: New York, 1983.
30. Elliott, S. R. *Physics of Amorphous Materials*, 2nd ed.; Longman Scientific and Technical: Essex, England, 1990.
31. Cody, V. *Endocrine Res.* **1985**, *11*, 211–224.
32. Shirke, S. M.S. Thesis, Rutgers, The State University of New Jersey, New Brunswick, NJ, 2005.
33. Roos, Y. H. *Carbohydr. Res.* **1993**, *238*, 39–48.
34. Orford, P. D.; Parker, R.; Ring, S. G. *Carbohydr. Res.* **1990**, *196*, 11–18.
35. Noel, T. R.; Parker, R.; Ring, S. G. *Carbohydr. Res.* **1996**, *282*, 193–206.
36. Noel, T. R.; Parker, R.; Ring, S. M.; Ring, S. G. *Carbohydr. Res.* **1999**, *319*, 166–171.
37. Noel, T. R.; Parker, R.; Ring, S. G. *Carbohydr. Res.* **2000**, *329*, 839–845.
38. Lebrun, N.; Van Miltenburg, J. C. *J. Alloys Compd.* **2001**, *320*, 320–325.
39. Carpentier, L.; Descamps, M. *J. Phys. Chem. B* **2003**, *107*, 271–275.
40. Maroncelli, M.; Fleming, G. R. *J. Chem. Phys.* **1987**, *86*, 6221–6239.
41. Duchowicz, R.; Ferrer, M. L.; Acuna, A. U. *Photochem. Photobiol.* **1998**, *68*, 494–501.
42. Lettinga, M. P.; Zuilhof, H.; van Zandvoort, A. M. J. *Phys. Chem. Chem. Phys.* **2000**, *2*, 3697–3707.
43. Crowe, J. H.; Carpenter, J. F.; Crowe, L. M. *Ann. Rev. Physiol.* **1998**, *60*, 73–103.